SPH MODELLING OF 3D BODY TRANSPORT IN FREE SURFACE FLOWS

Amicarelli A., Agate G., Guandalini R.
ASV - Environment and Sustainable Development
RSE Research on Energy Systems, Milan, Italy
Andrea.Amicarelli@rse-web.it
Giordano.Agate@rse-web.it
Roberto.Guandalini@rse-web.it

R. Albano, D. Mirauda, A. Sole
School Of Engineering
UNIBAS University of Basilicata, Potenza, Italy
albano.raffaele@tiscali.it
domenica.mirauda@unibas.it
aurelia.sole@unibas.it

***Abstract* - A 3D SPH numerical scheme has been developed to model the dynamics of rigid bodies, driven by free surface flows. It is based on the Euler-Newton equations for body dynamics, implemented using the SPH formalism. The scheme has been coupled to a Weakly Compressible SPH model for the main flow.**

The "fluid-body" 2-way coupling terms are modelled through an advanced SPH technique for boundary treatment (Adami et al., 2012), here adapted for free-slip conditions. The "solid-solid" ("body-body" and "body-frontier") 2-way coupling terms are represented using the boundary force particles described in Monaghan (2005). This technique has been modified, in order to model the impingements of entire bodies, even at low velocities.

The resulting numerical model is here validated on a 2D asymmetric wedge fall on still water and a 3D dam break event with transport of a floating body. This last phenomenon has also been experimentally realized during this study. Validation is analyzed by comparisons with measurements, URANS results and theoretical solutions.

I. INTRODUCTION

Body transport in free surface flows interests several application fields: flood events with transport of mobile structures, interaction of surface waves with floating bodies (e.g. buoys, platforms), ice floes, transport of tree trunks or branches in rivers or streams and their interactions with hydraulic constructions, etc..

Several SPH studies have dealt with the transport of solid bodies, driven by free surface or confined flows, mainly in 2D and dealing with single 2-way interactions. They are briefly described in the following.

[17] use the ghost particle method to model a 2D dynamics of a falling wedge into still water. [14] model the interactions between water surface waves and fixed cylinders through the use of the so-called "boundary force particles". Using the same technique, [15] and [16] represent the "fluid-body" interaction terms to model a floating body, driven by surface waves. Adopting this kind of particles, [10] reproduce 2D modular bodies in confined flows. The boundary force particles are still applied in [11], where they also use repulsive forces in order to model "solid-boundary" interactions. [7] represent the transport of 2D bodies in confined visco-elastic flows, deriving a formulation similar to [1] for "fluid-solid" interactions, and repulsive forces, defined for "body-body" impingements. The same authors represent the transport of 2D bodies in confined flows in [8]. [3] model the 3D impact of a falling parallelepiped on still water using a model, which couples Finite Element Method (solid dynamics) with SPH modeling (for fluid particles). Finally [18] directly represent solid-solid interactions by approximating the exact formulation for the collision of two rigid bodies in 3D (using an SPH formalism).

In this context we have developed and validated a 3D SPH scheme for body transport in free surface flows. We have coupled it to an SPH model for the main flow. The formulation of the fluid-body interaction terms is based on an adaptation of the boundary technique of [1], whose original formulation was quantitatively validated on fixed frontiers in 2D. Here we apply a variant of it ([2]), in order to model free-slip conditions. Body-body and body-boundary impingements are represented according to the boundary force particles, as formulated by [12], adapted in [2] to treat whole solid bodies, even at low velocities.

The resulting RSE model has been validated on 2D and 3D reference test cases, where measures and Unsteady Reynolds-Averaged Navier-Stokes (URANS) numerical results and theoretical solutions are available. Finally, the numerical model is validated on a laboratory test case (Basilicata University), a dam break event with 3D body transport, which has been realized during this study.

After this introduction (Sec.I), Sec.II describes the numerical model, Sec.III the main validation tests and Sec.IV the overall conclusions.

II. NUMERICAL MODEL

This section synthetically describes the main features of the numerical model: the balance equations for fluid (A) and body (B) dynamics and then the 2-way interaction terms related to both fluid-body (C) and solid-solid (D) interactions, respectively. Full details are provided in [2].

A. SPH balance equations for fluid dynamics

The numerical scheme for the main flow is based on the semi-analytic approach for boundary treatment ("fluid-boundary" interactions), as described in [4].

According to this approach, the continuity equation takes the following form:

$$\frac{d\rho_0}{dt} = \sum_b \rho_b (u_{jb} - u_{j0}) W_b' \omega_b + 2\rho_0 \int_{V_h'} [(\underline{u}_w - \underline{u}_0)\cdot \underline{n}] W' dx^3 + \underline{C}_s \quad (1)$$

where ρ is density, $\underline{u}$ the velocity vector, W the kernel function, ω the particle volume, $\underline{n}$ the vector normal to the fluid domain boundary. The summation in (1) is performed over the neighbouring particles ("$_b$"). The integral is instead computed over the complement V_h' (to the spherical kernel support) of the truncated kernel support. The subscripts "$_0$" and "$_w$" refers to the computational particle and the frontier respectively. Einstein's notation applies for the subscript "$_j$". Finally $\underline{C}_s$ represents the coupling term for fluid-body interactions, described in Sec.II.C.

On the other hand the momentum (Euler) equation is assumed:

$$\begin{aligned} \left\langle \frac{du_i}{dt} \right\rangle_0 &= -\delta_{i3} g + \sum_b \left(\frac{p_b}{\rho_b^2} + \frac{p_0}{\rho_0^2} \right) W_b' m_b + 2\frac{p_0}{\rho_0} \int_{V_h'} \frac{\partial W}{\partial x_i} dx^3 \\ &- \frac{\delta_{i3} g}{\rho_0} \int_{V_h'} W'(\underline{x} - \underline{x}_0) dx^3 - \upsilon_M \sum_b \frac{m_b}{\rho_0 r_{0b}^2} (\underline{u}_b - \underline{u}_0)\cdot(\underline{x}_b - \underline{x}_0) \frac{\partial W}{\partial x_i}\bigg|_b + \\ &- 2\upsilon_M (u_{w,j} - u_{0,j}) \cdot \int_{V_h'} \frac{1}{r_{0b}^2} (\underline{x} - \underline{x}_0) \frac{\partial W}{\partial x_i} dx^3 + \underline{a}_s \end{aligned} \quad (2)$$

where δ_{ij} is Kronecker's delta, p pressure, g the gravity acceleration, ν_M the artificial viscosity ([12]), m the particle mass and $\underline{r}$ the relative distance between each pair of interacting particles. $\underline{a}_s$ represents the coupling term for fluid-body interactions, as described in Sec.II.C.

A linearized barotropic state equation completes the model:

$$p \cong c_{ref}^2 (\rho - \rho_{ref}) \quad (3)$$

B. SPH balance equations for rigid body transport

The body dynamics is ruled by Euler-Newton equations:

$$\frac{d\underline{u}_{CM}}{dt} = \frac{\underline{F}_{TOT}}{m_B}, \quad \frac{d\underline{x}_{CM}}{dt} = \underline{u}_{CM} \quad (4)$$

$$\frac{d\underline{\omega}_B}{dt} = \underline{\underline{I}}_C^{-1} \left[\underline{M}_{TOT} - \underline{\omega}_B \otimes \left(\underline{\underline{I}}_C \underline{\omega}_B \right) \right], \quad \frac{d\underline{\alpha}}{dt} = \underline{\omega}_B \quad (5)$$

$\underline{F}_{TOT}$ is the global force acting on the solid. $\underline{\omega}_B$ denotes the angular velocity of the computational body, $\underline{\alpha}$ is the vector of the angles lying between the body axis and the global reference system. $\underline{M}_{TOT}$ represents the global moment acting on the body and $\underline{\underline{I}}_C$ the matrix of its moment of inertia. The subscript "$_{CM}$" refers to the body centre of mass.

The global force is composed of several terms:

$$\underline{F}_{TOT} = \underline{G} + \underline{P}_f + \underline{T}_f + \underline{P}_s + \underline{T}_s, \qquad \underline{T}_f + \underline{T}_s \cong 0 \quad (6)$$

$\underline{G}$ represents the gravity force, while $\underline{P}_f$ and $\underline{T}_f$ the sum of the pressure and shear forces, provided by the fluid. Analogously $\underline{P}_s$ and $\underline{T}_s$ are the sum of the normal and the shear forces exerted by other bodies or boundaries (solid-solid interactions). Shear forces are here considered negligible.

The pressure hydrodynamic force on the body is:

$$\underline{P}_f = \sum_s p_s A_s \underline{n}_s \quad (7)$$

The computational body is numerically represented by solid volume elements, simply called (solid) body particles ("$_s$"). Some of them describe the body surface and are referred to as "surface body particles". These particular elements are also characterized by an area and a vector $\underline{n}$ of norm 1. This is perpendicular to the body face the particle belongs to and points outward the fluid domain (inward the solid body). The body particle pressure is computed as described in Sec.II.C.

The global moment is discretized as follows:

$$\underline{M}_{TOT} = \sum_s \underline{r}_s \otimes \underline{F}_s \quad (8)$$

while the body particle velocity is the vector sum of the body velocity and the relative velocity of the particle, with respect to the body centre of mass $(\underline{r}_s \equiv \underline{r}_{s,CM})$:

$$\underline{u}_s = \underline{u}_{CM} + \underline{\omega}_B \otimes \underline{r}_s \quad (9)$$

The body particle normal and position need to be updated every time step:

$$\underline{n}_s(t+dt) = \underline{\underline{R}}_B \underline{n}_s(t), \underline{x}_s(t+dt) = \underline{x}_{CM}(t+dt) + \underline{\underline{R}}_B \underline{r}_s(t) \quad (10)$$

according to the rotation matrix of the body R_{ij}, which in turn depends on the body orientation:

$$d\underline{\alpha}_B = \underline{\omega}_B dt \quad (11)$$

C. Fluid-body interaction terms

The fluid-body interaction terms rely on the boundary technique introduced by [1], here adapted for free-slip conditions.

The fluid-body interaction term, in the continuity equation (1), can be formulated as follows:

$$\underline{C}_s = 2\rho_0 \sum_s [(\underline{u}_s - \underline{u}_0)\cdot \underline{n}_s] W_s' \omega_s \quad (12)$$

and the analogous term in the momentum equation is written as

$$\underline{a}_s = \sum_s \left(\frac{p_s + p_0}{\rho_0^2} \right) W_s' m_s \qquad (13)$$

The pressure value of a generic neighbouring (surface) body particle "$_s$" can be derived:

$$p_s = \frac{\sum_0 \left[p_0 + \rho_0 \left(\underline{g} - \underline{a}_s \right) \cdot \left(\underline{r}_{s0} \cdot \underline{n}_s \right) \right] W_{0s} \left(\frac{m_0}{\rho_0} \right)}{\sum_0 W_{0s} \left(\frac{m_0}{\rho_0} \right)} \qquad (14)$$

where each fluid particle – body particle interaction is represented by the subscript "$_{s0}$".

D. Solid-solid interaction terms

The solid-solid interaction term in (6) represents a (full elastic) impingement force. For a body-body interaction it can be expressed as follows:

$$\underline{P}_s = -\alpha_I \sum_j \sum_k \frac{2u_{\perp,jk}^2}{r_{per,jk}} \frac{m_j m_k}{m_j + m_k} \Gamma_{jk} \left(1 - \frac{r_{par,jk}}{dx_s} \right) \underline{n}_k \qquad (15)$$

This force involves interactions between all the body particles "$_j$" of the computational body "$_B$" and their corresponding neighbour body particles "$_k$", belonging to all the other bodies. The direction of a generic partial force, related to each particle-particle interaction, is aligned with the normal of the neighbour particle. Its magnitude depends on particle masses, the relative position of the interacting particles, the impact velocity $u_\perp$ and the normalizing factor α_I. r_{par} and r_{per} are parallel and the perpendicular components of the relative distance between the two interacting particles, respectively. The term within brackets in (15) deforms the kernel support of the body particles "$_j$", so that it only develops aligned with the normal of the neighbouring particle (dx_s represents the size of the body particles). Γ is a further weighting function, different from W.

The impact velocity is computed as the maximum value of the relative velocity (projected over the normal of the neighbouring particle), estimated over all the body particle interactions during the whole duration of the approaching phase $(t_0 \le t \le t_a)$ of the impingement:

$$u_{\perp,jk} = \max_{j,k,t} \left\{ \left| \left(\underline{u}_j - \underline{u}_j \right) \cdot \underline{n}_k \right| \right\}, \qquad t_0 \le t \le t_a \qquad (16)$$

α_I is a normalizing parameter which allows treating whole solid bodies, instead of particle-particle impingements:

$$\alpha_I = \sum_K \frac{1}{r_{per,BK}} \frac{m_B m_K}{m_B + m_K} \Gamma_{BK} \Big/ \sum_j \sum_k \left[\frac{1}{r_{per,jk}} \frac{m_j m_k}{m_j + m_k} \Gamma_{jk} \left(1 - \frac{r_{par,jk}}{dx_s} \right) \right] \qquad (17)$$

with the subscript "$_K$" denoting a generic neighbouring body.

On the other hand we need to model body-boundary interactions. In this frame we can consider the boundary as a body with infinite mass and discretization tending to zero (the semi-analytic approach, we use to model fixed frontiers, is in fact an integral method). The interaction force then becomes:

$$\underline{P}_s = -\alpha_I \sum_j \sum_k \frac{2u_{\perp,jk}^2}{r_{per,jk}} m_j \Gamma_{jk} \underline{n}_k, \alpha_I = \frac{m_B}{r_{per,Bk}} \Gamma_{Bk} \Big/ \sum_j \sum_k \left[\frac{m_j}{r_{per,jk}} \Gamma_{jk} \right] \qquad (18)$$

with the subscript "$_k$" here denoting a neighbouring frontier.

III. RESULTS

The two validation test cases here explored refer to a 2D wedge fall on still water (Sec.III.A) and a dam break event (Sec.III.B), involving the 3D transport (6 degrees of freedom) of a floating body, a moving dam/gate (treated as a body in terms of fluid-body interactions) and fixed obstacles (treated as frontiers). For both these test cases we set h/dx=1.3 and CFL=0.1. If not otherwise stated, the present model will be denoted by "SPH-body", just for simplicity of notation. For further investigations and validations on the presented model we refer to [2].

A. Solid wedge falling on still water (2D)

This section describes the validation test case representing the asymmetric falling of a medium (weight) wedge ([9], Fig.1d).

The height of the body centre of mass at the beginning of the phenomenon is $z_{CM}(t0)$=(0.165+0.610)m. Its mass and moment of inertia are m_B=120.080kg/m and I_c=4.4877kg*m, respectively. The heel angle (at t_0) is 5°. The impact time is t_{imp}=0.355s.

As we just perform a single phase simulation, we consider that, before the impact with water, the wedge simply falls according to gravity. This hypothesis introduces some discrepancies with respect to the experiment, mainly in terms of initial conditions of the very numerical simulations, which start at the impact time (t_{imp}), provided as an experimental input. The base of the triangular wedge (Fig.1-d) is L=0.610m, its height H=0.111m. The origin of the reference system is located where the lowest point of the solid triangle touches the free surface at t_{imp}. The numerical simulation uses dx=0.002m and dx/dx_s=2.0. Even if the impact time is an experimental input, some minor discrepancies still survive in terms of numerical initial conditions. In fact our mono-phase approach determines an impact velocity of -3.459m/s and the wedge orientation should not change during the fall. We cannot replace these data with the experimental ones, because they are not available. However this lack of data, even if appreciable, is not relevant for this test, as demonstrated in [2].

Validations are performed against experimental results ([9]) in terms of vertical acceleration, normalized by g (a/g), and

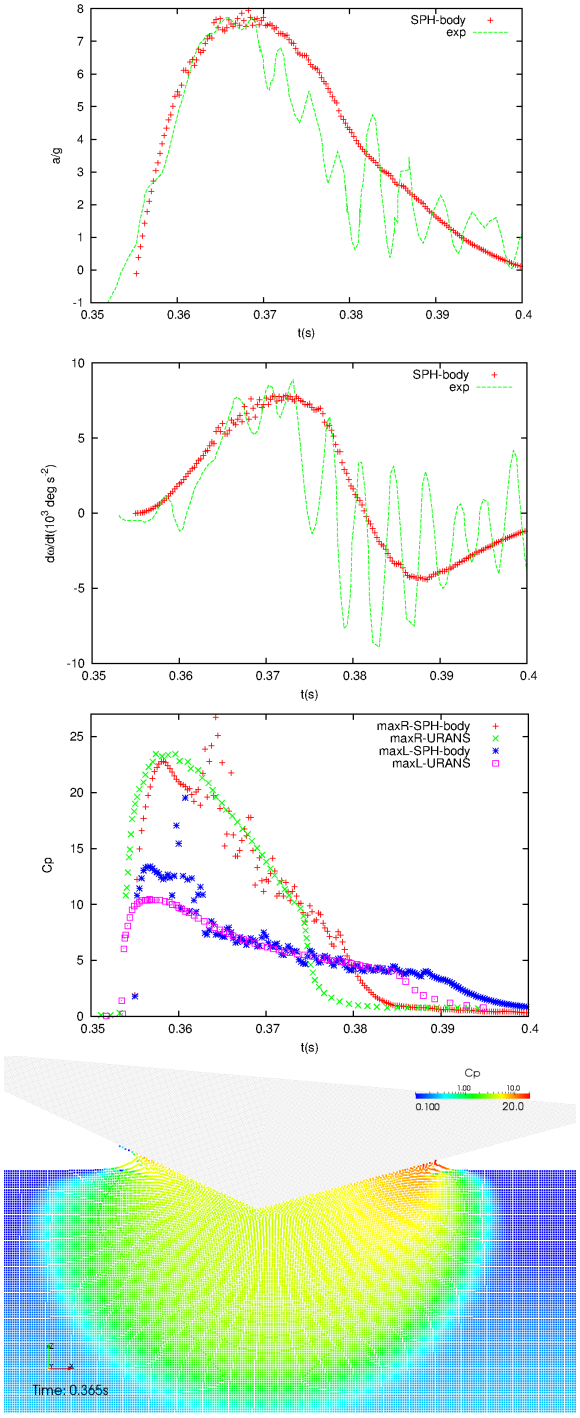

Figure 1. Asymmetric medium wedge. Validation and inter-comparisons. From top to bottom. (a) Time evolution of the normalized acceleration. (b) Time evolution of the angular acceleration. (c) Time evolution of the maximum value of the pressure coefficient over the wedge. (d) Example of the field of the pressure coefficient.

angular acceleration, expressed in 10^3degrees/s. Further inter-comparisons are provided for the maximum values of pressure on the wedge sides, by icomparison with URANS results ([9]).

Fig.1 shows the comparisons between the numerical and experimental values of the normalized acceleration (-a-) and the angular acceleration (-b-). The first is well reproduced in terms of time evolution and peak value. The angular acceleration is still well represented, by correctly filtering the small scale oscillations (due to the body deformability), which are beyond the scope of this study and cannot be modelled within the frame of rigid body dynamics.

Time evolution of the maximum values of the pressure coefficient, on both the right (R) and left (L) sides of the wedge, is satisfactorily reproduced (Fig.1-c), although some overestimations in the left side values, with respect to the URANS data, as well as some noise in the curve evolution.

Finally an example of the field of the pressure coefficient is shown in Fig.1-d. At this time the left vertex of the wedge begins to impact the water pool. The spatial evolution of C_p is regular and allows avoiding penetrations of fluid particles into the solid body (here coloured in transparent black).

B. Dam break with transport of a floating body (3D)

The model described in Sec.II has been validated on a 3D experimental dam break event, which involves the transport of a floating body and its interactions with two fixed obstacles, a mobile gate (representing a dam) and fixed frontiers.

The experimental tests have been carried out in the Hydraulics Laboratory of Basilicata University, on a channel characterized by a rectangular cross section of 0.5m in width and 0,6m in height. An automatic mechanism regularly opens the gate, so quickly to obtain an event as possible similar to a dam-break. The experiment provides some measurements of the body trajectory and free surface levels close to the two fixed obstacles. The phenomenon represents the evolution of a dam break front, as resulting from a regular (non-instantaneous) lifting of a gate, which initially confines the water reservoir. This experimental configuration seems more complex than others available in literature (e.g. [6] and [19]), because it considers more than one fixed obstacle and a transported floating body.

The gate begins to lift a $t=t_0=2.00$s, with a uniform vertical velocity w=0.11m/s until t=5.00s, when it stops. Further the estimated parameters are normalized assuming the velocity scale as $\sqrt{2gH}$ =2.646s. The domain and the water reservoir dimensions are 3.500x0.500x0.500 m^3 and 0.500x0.500x0.350 m^3, respectively (Fig.2). The dimension of each obstacle is 0.150x0.150x0.750m^3. The first ("obstacle 1") is 2.5m distant from the left boundary of the domain. The same distance measures 2.950m for the down-flow obstacle ("obstacle 2"). Both are 0.060m far from their closest vertical boundary (lateral wall of the channel). The transported body is a cube with side 0.054m, mass m_B=0.073kg, (ρ_s=464kg/m^3). The body centre of mass is initially at rest and is located 2.532m far from the left boundary of the reservoir, 0.313m from the right wall and 0.027m from the bottom, where the body lies on. We prefer to optimize the initial position of the body by displacing of a very little quantity (smaller than the spatial resolution of the model) its initial y-coordinate, in order to provide the best initial conditions to the body dynamics, without deteriorating

the model resolution. The gate is also modelled as a numerical body (not a frontier), but its kinematics is imposed. The gate size is 0.0376x0.500x0.400m^3. We numerically set dx/dx_s=5/3, with dx=0.0125m.

Fig.2 reports an example of the field of the absolute value of the normalized velocity (lateral view), after the first impact of the body.

Fig.3 provides a graphical comparison between the numerical and the experimental positions of the body. It approaches the obstacles (t=3.25s), impinges on it (at around t=3.50s), is transported within the recirculation region up-flow the obstacle (t=3.75s), deviates laterally (t=4.00s) and begins to overpass it (t=4.35s). The model can correctly reproduce the body trajectory, even if the body dynamics is strongly non-linear in the recirculation zone around the "obstacle 2".

Fig.4 provides quantitative comparisons between the numerical results and the experimental data, in terms of body trajectory and free surface levels. The time evolution of the x-component of the centre of mass position is well reproduced by the model (a). The body begins to move at around 3.2s and impacts the second obstacle. Between t=3.4s and t=4.0s the body is entrained in the recirculation region. It then deviates laterally and reaches a zone at low velocities, close to the down-flow frontier. At around t=5.5s it begins to move backward, transported by the main flow, while a reflected front wave move towards the gate. Some minor errors are still detectable, as the numerical body begins to move back a little earlier.

The experimental data concerning the vertical position of the body are reported in Fig.3 (b). Their experimental errors are not negligible, as shown in the figure. Nevertheless a comparison can be performed and the numerical results reveal to be in good agreement with respect to the experimental time evolution. The vertical position of the floating body is normally related to the position of the free surface at those horizontal coordinates. However, just after the first impact, the body moves in air (at around t=3.6s) after its impact against the down-flow obstacle.

IV. Conclusions

We have developed and validated an SPH model for the 3D transport of solid bodies in free surface flows. It solves the balance equations for the 3D dynamics of rigid bodies and involves fluid-body and solid-solid multiple interactions. The fluid-body interactions are modelled according to the boundary treatment introduced by [1], validated in 3D and adapted ([2]) to handle free-slip conditions. The solid-solid multiple interactions (body-body and body-boundary impingements) are represented using the SPH boundary force particles of [12], adapted ([2]) to deal with low velocity impingements of entire solid bodies. This numerical scheme for body dynamics has been coupled to a Weakly Compressible SPH model, which is based on the semi-analytic approach for treating the "fluid-boundary" interactions, as described in ([4]).

The numerical model is here validated on a 2D asymmetric fall of a solid wedge into still water and a 3D dam break event with fixed obstacles, a mobile gate/dam and a transported floating

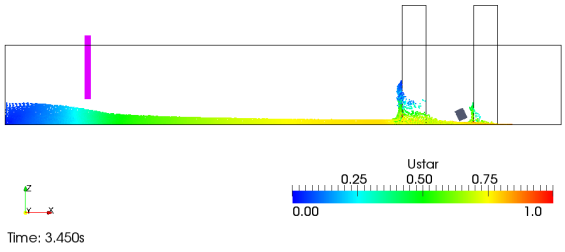

Figure 2. Dam break with 3D body transport. Absolute value of the normalized velocity at t=3.45s (lateral view).

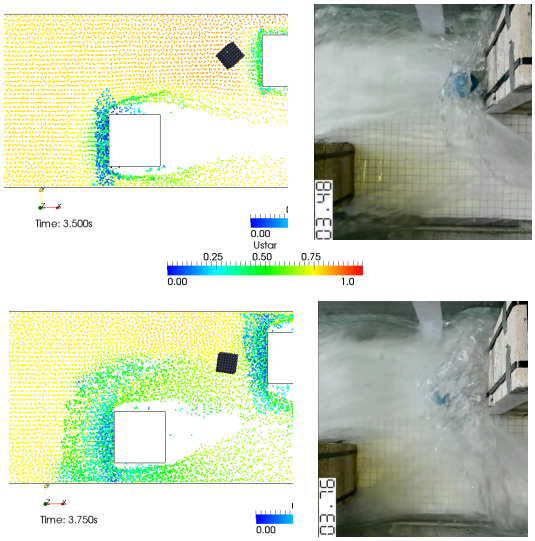

Figure 3. Dam break with 3D body transport (numeration from left to right). Examples of graphical comparisons of the body trajectory between the SPH simulation and the experiment at t=3.5s (top) and t=3.75s (bottom).

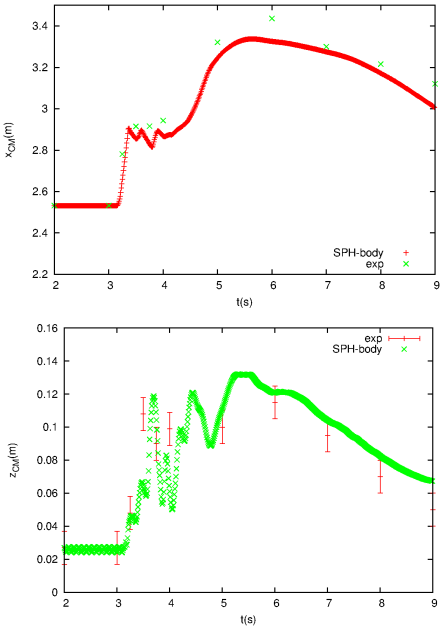

Figure 4. Time evolution of the x (top: a) and z (bottom: b) coordinates of the body barycentre (SPH vs measures).

body. This last phenomenon has been both numerically and experimentally realized during this study.

These validations, performed by comparisons with experimental and URANS data, show the reliability of the model in representing the transport of solid bodies in 3D free surface flows, with simultaneous fluid-body and solid-solid interactions. Related application fields are: transport of solid structures and bodies during floods, river overflows or tsunami events; interactions of surface waves with floating bodies, ice floes, hydraulic turbines, impacts of falling bodies (e.g. aircraft ditching).

ACKNOWLEDGEMENTS

This work has been financed by the Research Fund for the Italian Electrical System under the Contract Agreement between RSE S.p.A. and the Ministry of Economic Development - General Directorate for Nuclear Energy, Renewable Energy and Energy Efficiency in compliance with the Decree of March 8, 2006.

REFERENCES

[1] Adami S., X. Y. Hu, N. A. Adams; 2012; A generalized wall boundary condition for smoothed particle hydrodynamics; Journal of Computational Physics, 231, 7057–7075.

[2] Amicarelli A., R. Albano, D. Mirauda, G. Agate, A. Sole, R. Guandalini; A Smoothed Particle Hydrodynamics model for 3D solid body transport in inertial free surface flows; in revision; International Journal for Numerical Methods in Engineering.

[3] Anghileri M., L.-M. L. Castelletti, E. Francesconi, A. Milanese, M. Pittofrati; Rigid body water impact - experimental tests and numerical simulations using the SPH method (2011); International Journal of Impact Engineering; 38, 141-151.

[4] Di Monaco A., Manenti S., Gallati M., Sibilla S., Agate G., Guandalini R., 2011; SPH modeling of solid boundaries through a semi-analytic approach; Engineering Applications of Computational Fluid Mechanics, 5, 1, 1–15.

[5] Ferrand M., D.R. Laurence, B.D. Rogers, D. Violeau, C. Kassiotis; 2012; Unified semi-analytical wall boundary conditions for inviscid laminar or turbulent flows in the meshless SPH method; Inetrnational Journal for Numerical Methods in Fluids; Published online (wileyonlinelibrary.com).

[6] Gómez-Gesteira M., R.A. Dalrymple; 2004; Using a 3D SPH Method for Wave Impact on a Tall Structure; J. Waterways, Port, Coastal, Ocean Engineering, 130/2, 63-69.

[7] Hashemi M. R., R. Fatehi, M. T. Manzari; SPH simulation of interacting solid bodies suspended in a shear flow of an Oldroyd-B fluid (2011); Journal of Non-Newtonian Fluid Mechanics, 166, 1239–1252.

[8] Hashemi M. R., R. Fatehi, M. T. Manzari; A modified SPH method for simulating motion of rigid bodies in Newtonian fluid flows (2012); International Journal of Non-Linear Mechanics, 47, 626–638.

[9] Hay A., A. Leroyer, M. Visonneau; H-adaptive Navier–Stokes simulations of free-surface flows around moving bodies (2006); J Mar Sci Technol, 11, 1–18.

[10] Kajtar J. B.; Monaghan J. J.; On the dynamics of swimming linked bodies (2010); European Journal of Mechanics B/Fluids, 29, 377-386.

[11] Kajtar J. B.; Monaghan J. J.; On the swimming of fish like bodies near free and fixed boundaries (2012); European Journal of Mechanics B/Fluids, 33, 1–13.

[12] Monaghan J.J.; 2005; Smoothed particle hydrodynamics; Rep. Prog. Phys. 68, 1703–1759.

[13] Monaghan J.J., J.B. Kajtar; 2009; SPH particle boundary forces for arbitrary boundaries; Computer Physics Communications, 180, 1811–1820.

[14] Monaghan JJ, Kos A, Issa N.; 2003; Fluid motion generated by impact. Journal of Waterway, Port, Coastal and Ocean Engineering; 129:250–259.

[15] Omidvar P., P. K. Stansby, B. D. Rogers; 2012; Wave body interaction in 2D using smoothed particle hydrodynamics (SPH) with variable particle mass; Int. J. Numer. Meth. Fluids; 68:686–705.

[16] Omidvar P., P. K. Stansby, B. D. Rogers; 2012; SPH for 3D floating bodies using variable mass particle distribution; Int. J. Numer. Meth. Fluids, DOI: 10.1002/fld.3749

[17] Oger G., M. Doring, B. Alessandrini, P. Ferrant; 2006; Impulse-based rigid body interaction in SPH; Journal of Computational Physics, 213, 803–822.

[18] Seungtaik Oh, Younghee Kim, Byung-Seok Roh; Impulse-based Boundary Force (IBF); 2009; Computer Animation and Virtual Worlds; Comp. Anim. Virtual Worlds, 20, 215–224.

[19] Soares-Frazão S.A., Zech Y.; 2007; Experimental study of dam-break flow against an isolated obstacle; Journal of Hydraulic Research, 45, Supplement 1, 27-36.